BIOCHEMICAL PHARMACOLOGY 76 (2008) 156–168

available at www.sciencedirect.com

ScienceDirect

journal homepage: www.elsevier.com/locate/biochempharm

Selective targeting of the HIV-1 reverse transcriptase catalytic complex through interaction with the "primer grip" region by pyrrolobenzoxazepinone non-nucleoside inhibitors correlates with increased activity towards drug-resistant mutants

Samantha Zanoli [a], *Sandra Gemma* [b,e], *Stefania Butini* [b,e], *Margherita Brindisi* [b,e], *Bhupendra P. Joshi* [b,e], *Giuseppe Campiani* [b,e], *Caterina Fattorusso* [c,e,*], *Marco Persico* [c,e], *Emmanuele Crespan* [a], *Reynel Cancio* [a], *Silvio Spadari* [a], *Ulrich Hübscher* [d], *Giovanni Maga* [a,e,**]

[a] *Institute of Molecular Genetics, IGM-CNR, via Abbiategrasso 207, I-27100 Pavia, Italy*
[b] *Dipartimento Farmaco Chimico Tecnologico, Universita' degli Studi di Siena, via Aldo Moro, I-53100 Siena, Italy*
[c] *Dipartimento di Chimica delle Sostanze Naturali, Universita' di Napoli "Federico II", via D. Montesano 49, I-80131 Napoli, Italy*
[d] *Institute of Veterinary Biochemistry and Molecular Biology, University of Zürich-Irchel, CH-8057 Zürich, Switzerland*
[e] *European Research Centre for Drug Discovery and Development, Universita' degli Studi di Siena, I-53100 Siena, Italy*

ARTICLE INFO

Article history:
Received 13 March 2008
Accepted 11 April 2008

Keywords:
HIV-1
Reverse transcriptase
NNRTIs
Kinetics
Drug resistant
Molecular modeling

ABSTRACT

PBO (pyrrolobenzoxazepinone) derivatives are non-nucleoside reverse transcriptase inhibitors (NNRTIs), which display a selective interaction with the catalytic ternary complex of HIV-1 reverse transcriptase (RT) and its substrates. In order to develop novel PBOs with improved resistance profiles, we synthesised additional PBO derivatives, specifically designed to target highly conserved residues in the β12–β13 hairpin, the so-called "primer grip" region of HIV-1 RT. Here, we investigated the biochemical and enzymological mechanism of inhibition of HIV-1 RT wild type and carrying NNRTIs-resistance mutations, by these derivatives. Our kinetic analysis indicates that the ability of PBOs to selectively target the catalytic ternary complex of RT with its substrates directly correlates with greatly reduced sensitivity to NNRTIs-resistance mutations, particularly the K103N substitution. Molecular modeling and docking studies provided an explanation for this correlation at the structural level.

1. Introduction

Non-nucleoside reverse transcriptase inhibitors (NNRTIs) are allosteric and non-competitive modulators of reverse transcriptase (RT), one of the key enzyme in the life cycle of HIV-1 [1,2]. Because of their generally good tolerability and low toxicity [3], these drugs are essential components of highly active antiretroviral therapy (HAART), with nucleoside reverse

* *Corresponding author at*: Dipartimento di Chimica delle Sostanze Naturali, Universita' di Napoli "Federico II", via D. Montesano 49, I-80131 Napoli, Italy.
** *Corresponding author at*: Institute of Molecular Genetics, IGM-CNR, via Abbiategrasso 207, I-27100 Pavia, Italy. Tel.: +39 0382546354; fax: +39 0382422286.
E-mail addresses: cfattoru@unina.it (C. Fattorusso), maga@igm.cnr.it (G. Maga).
0006-2952/$ – see front matter © 2008 Elsevier Inc. All rights reserved.
doi:10.1016/j.bcp.2008.04.009

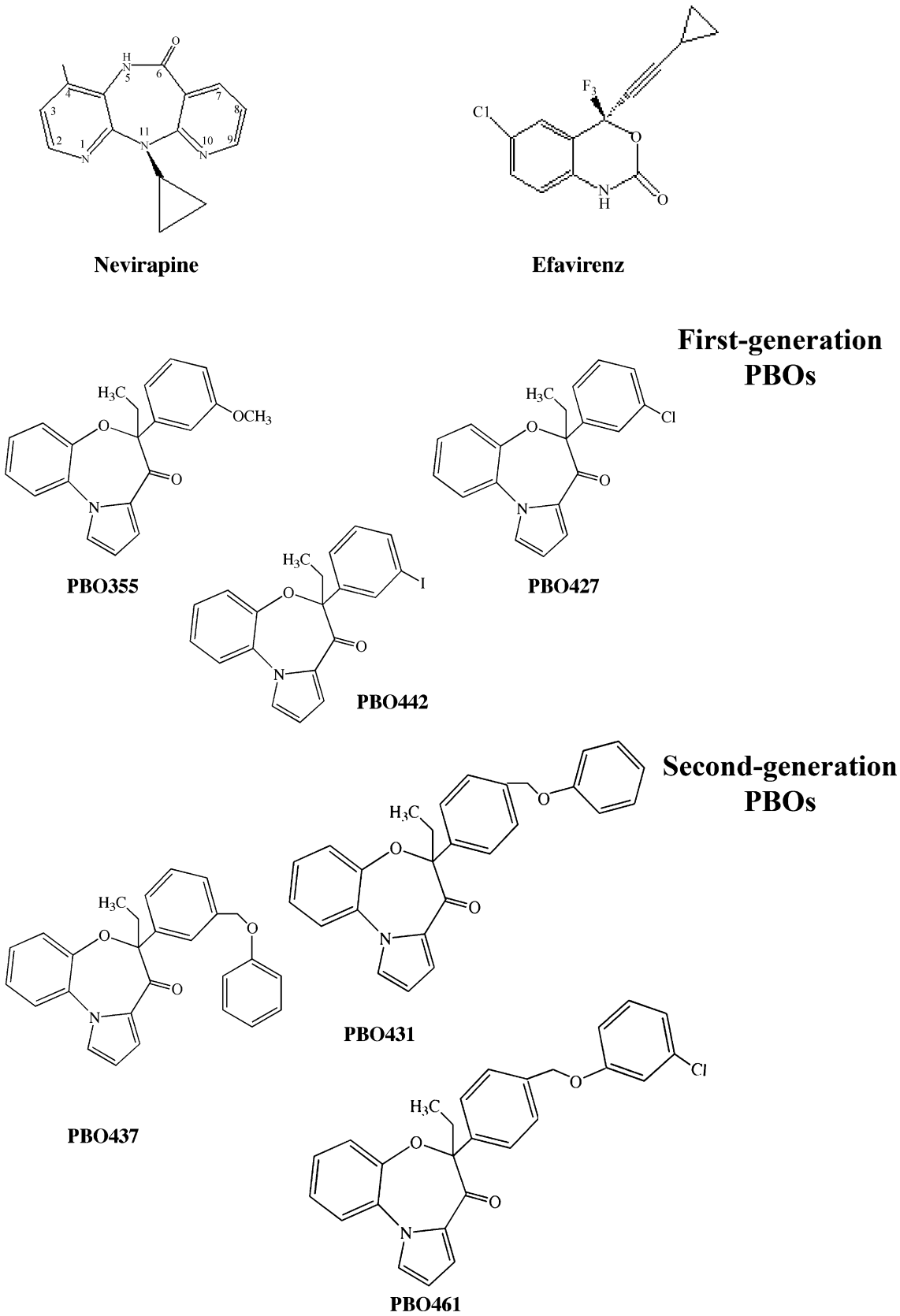

Fig. 1 – Structures of the NNRTIs nevirapine and efavirenz and of the PBO derivatives used in this study.

transcriptase inhibitors (NRTI) and/or protease inhibitors (PI). The multidrug therapy provides a substantial delay in disease progression compared to monotherapy or dual therapy, allowing significant immune system function restoration, and retarding the emergence of resistant viral strains [3,4]. So-called ''first-generation'' NNRTI drugs, such as nevirapine (Fig. 1), are generally very susceptible to the effects of a single critical amino acid change in the NNRTI binding pocket [5]; in contrast, the more recent ''second''- and ''third-generation'' NNRTIs (e.g. efavirenz, etravirine, rilpivirine, dapivirine) are characterised by a more favourable profile of resilience to common resistance mutations [6]. However, the possible development of resistance, and especially cross-resistance to such compounds, with reduction of therapeutic options in the case of unsuccessful regimens, accounts for a continue development of new, potent, broad-spectrum NNRTI antiviral agents [7].

In a previous paper [8] we reported a series of PBO (pyrrolobenzoxazepinone) derivatives as novel NNRTIs. Further characterization revealed a novel mechanism of action for some derivatives belonging to this class of compounds, namely a selective interaction with the catalytic ternary complex of RT and its substrates resulting in strong synergy with other NRTIs and NNRTIs [9]. Although first-generation PBOs were still hampered by common NNRTIs-resistance mutations, enzymological studies highlighted the correlation between the selective targeting of the ternary complex and their resistance profile. In fact, one mutation (L100I), resulted in PBO resistance specifically due to a reduced affinity of the molecules for the ternary complex of this mutant [9]. In order to develop potential drugs with improved resistance profiles for chronic use in anti-HIV combination therapy, we focused our efforts on the identification of those structural requirements responsible for high activity toward a wide range of HIV-1 variants [10]. The rationale used was that binding of NNRTIs at highly conserved amino acid residues in the NNRTI binding pocket, which are essential for correct enzyme functioning and for viral replication and thus unlike to mutate under drug pressure, could result in the development of novel NNRTIs selectively targeting the RT ternary complex and not sensitive to common enzyme mutations, as those occurring at Y181, L100, and K103 residues. We identified three highly conserved residues, F227, W229, L234, which are part of the β12–β13 hairpin (F227-H235), the so-called ''primer grip'', responsible for maintaining the primer terminus in the appropriate orientation for nucleophilic attack on an incoming dNTP. Mutations in this region, including the conservative mutations W229F and W229Y, significantly compromise RNA- and DNA-dependent DNA polymerase activities of RT [11,12]. Accordingly, mutation of the key residue W229 has never been observed in combination to other mutations, during therapy with NNRTIs. Within the first generation of PBOs, we have been able to identify the analogues PBO355, PBO427, and PBO442 (Fig. 1) as potent NNRTIs. Subsequently, their structure has been rationally modified with the aim to target the highly conserved amino acid residues within the β12–β13 hairpin (F227, W229, M230), leading to the development of additional PBO NNRTIs (PBO 431, PBO437, PBO461) [10]. These compounds were shown to potently inhibit HIV-1 replication in cultured cells [10], but a detailed study of their mechanism of action was still lacking. In the present manuscript, we investigated the biochemical and enzymological mechanism of inhibition of HIV-1 RT wild type and carrying NNRTIs-resistance mutations, by the optimized derivatives PBO431, PBO437 and PBO461 in comparison to the PBO355, PBO427 and PBO442 (Fig. 1). Our kinetic analysis indicates that the ability of PBOs to selectively target the catalytic ternary complex of RT with its substrates directly correlates with greatly reduced sensitivity to NNRTIs-resistance mutations, particularly the K103N substitution. Molecular modeling and docking studies provided an explanation for this correlation at the structural level.

2. Material and methods

2.1. Inhibitors

The PBO derivatives shown in Fig. 1 were synthesized as previously described [8,10]. AZDTTP was from Amersham Biosciencies.

2.2. Nucleic acid substrates

The homopolymers poly(rA) or poly(dA) (Amersham Biosciencies) were mixed at weight ratios in nucleotides of 10:1, to the oligomer oligo(dT)12–18 (Amersham Biosciencies) in 20 mM Tris–HCl (pH 8.0), containing 20 mM KCl and 1 mM EDTA, heated at 65 °C for 5 min and then slowly cooled at room temperature.

2.3. Expression and purification of recombinant HIV-1 RT forms

The coexpression vectors pUC12N/p66(His)/p51with the wild type HIV-1 RT p66/p51 or the point mutants L100Ip66/p51 and V106Ap66/p51 [13] were kindly provided by Dr. S. H. Hughes (NCI-Frederick Cancer Research and Development Center) and purified in two steps as described [14,15]. Recombinant RT was purified to >95% purity and had a specific activity on poly(rA)/oligo(dT) (see below) of 75670 U/mg for RT wild type, 56,690 U/mg for RT L100I and 62,760 U/mg for RT V106A; 1 unit of DNA polymerase activity corresponds to the incorporation of 1 nmol of dNMP into acid-precipitable material in 60 min at 37 °C. The identity of the introduced mutations was confirmed by sequencing [13].

2.4. HIV-1 DNA polymerase activity assay

RNA- or DNA-dependent DNA polymerase activity was assayed as follows: a final volume of 25 μl contained buffer A (50 mM Tris–HCl pH 7.5, 1 mM DTT, 0.2 mg/ml BSA, 4% glycerol), 10 mM $MgCl_2$, 0.5 μg of either poly(rA)/oligo(dT)$_{1:10}$ or poly(dA)/oligo(dT)$_{1:10}$ (0.3 μM 3′-OH ends), [3H]-dTTP (1 Ci/mmol) as indicated in the figure legends and 2–4 nM RT. Reactions were incubated at 37 °C for the indicated time. When activated DNA was used, [3H]-dNTPs (4 Ci/mmol) were added in place of dTTP, in the presence of 0.04 mg/ml of the DNA template. 20 μl aliquots were then spotted on glass fiber filters GF/C which were immediately immersed in 5% ice-cold TCA. Filters were washed twice in 5% ice-cold TCA and once in

ethanol for 5 min, dried and acid-precipitable radioactivity was quantitated by scintillation counting.

2.5. Inhibition assays

Reactions were performed under the conditions described for the HIV-1 RT RNA- or DNA-dependent DNA polymerase activity assay. Incorporation of radioactive dTTP into poly(rA)/oligo(dT) or poly(dA)/oligo(dT) at different concentrations of dTTP was monitored in the presence of increasing amounts of inhibitor as indicated in the figure legends.

2.6. Kinetics of inhibitor binding

HIV-1 RT (20–40 nM) was incubated 2 min at 37 °C in a final volume of 4 μl in the presence of Buffer A, 10 mM $MgCl_2$, 100 nM 3′-OH ends and 10 μM unlabelled dTTP (for the formation of the RT/TP/dNTP complex). The inhibitor to be tested was then added to a final volume of 5 μl, at a concentration at which $[EI]/[E_0] = (1 - 1/(1 + [I]/K_i)) > 0.9$. Then, 145 μl of a mix containing Buffer A, 10 mM $MgCl_2$ and 10 μM [3H]-dTTP (5 Ci/mmol) were added at different time points. After additional 10 min of incubation at 37 °C, 50-μl aliquots were spotted on GF/C filters and acid-precipitable radioactivity measured as described for the HIV-1 RT RNA-dependent DNA polymerase activity assay. The quantity (v_t/v_0) representing the normalized difference between the amounts of [^{3}H]-dTTP incorporated in the nucleic acid substrate at the zero time point (v_0) and at the different time points (v_t) was then plotted against time.

2.7. Kinetic parameters calculation

All values were calculated by non-least squares computer fitting of the experimental data to the appropriate rate equations. K_m and k_{cat} values were calculated according to the Michelis–Menten equation, by analysing the variation of the initial velocities of the reaction in dependence of the substrate concentration. Time-dependent incorporation of

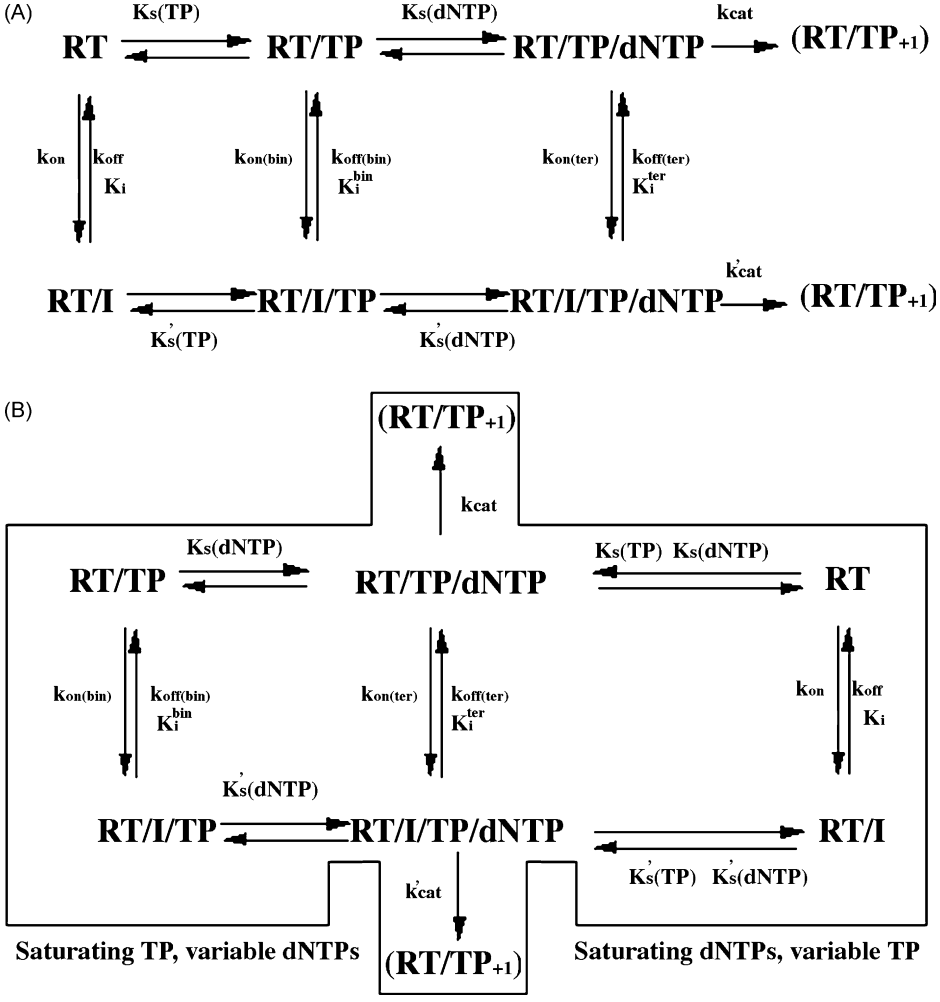

Scheme 1 – Simplified kinetic pathway for the reaction catalysed by HIV-1 RT and its interaction with inhibitors. (A) Schematic representation of the different equilibria in the reaction catalysed by HIV-1 RT in the absence or in the presence of an inhibitor. TP, template/primer; dNTP, nucleoside triphosphate; I, inhibitor; K_m, Michelis constant relative to the different substrates; k_{cat}, apparent catalytic rate; k_{off}, dissociation rate; k_{on}, association rate; K_i, equilibrium dissociation constant of the inhibitor; bin, binary complex of the enzyme with the TP substrate; ter, ternary complex of the enzyme with the TP and dNTP substrates. (B) Simplified reaction pathway under the reaction conditions used in this study. For details see text.

radioactive dTTP into poly(rA)/oligo(dT) at different substrate concentrations was monitored by removing 20 μl aliquots at 2 min, 4 min, 6 min, 12 min time points. Initial velocities of the reaction, determined by linear regression analysis of the data, were then plotted against the corresponding substrate concentrations.

According to the ordered mechanism of the polymerization reaction, whereby template–primer (TP) binds first followed by the addition of dNTP, HIV-1 RT can be present in three different catalytic forms as reported in Scheme 1A: as a free enzyme, in a binary complex with the TP, and in a ternary complex with TP and dNTP. The resulting rate equation for such a system is very complex and impractical to use. For these reasons, the general steady-state kinetic analysis was simplified by varying one of the substrates (either TP or dNTP) while the other was kept constant. When the TP substrate was held constant at saturating concentration and the inhibition at various concentrations of dNTPs was analyzed, at the steady-state all of the input RT was in the form of the RT/TP binary complex and only two forms of the enzyme (the binary complex and the ternary complex with dNTP) could react with the inhibitor, as shown in the left part of Scheme 1B. Similarly, when the dNTP concentration was kept constant at saturating levels and the inhibition at various TP concentrations was analyzed, RT was present either as a free enzyme or in the ternary complex with TP and dNTP, as shown in the right part of Scheme 1B.

K_i^{free} and K_i^{bin} values for the free enzyme or the binary complex were calculated according to the equation:

$$v = \left(\frac{V_m/(1+[I]/K_d)}{(1+(K_m/[S])((1+[I]/K_d)/(1+[I]/K'_d)))}\right) \quad (1)$$

where $K_d = K_i^{free}$ at constant dNTP and variable template–primer (TP), or K_i^{bin} at constant TP and variable dNTP. $K'_d = K_i^{ter}$ in both cases.

The equilibrium dissociation constant for the ternary complex (K_i^{ter}) was calculated from the variation of K_{app} (defined as the concentration of inhibitor reducing the RT activity by 50% at any given dTTP concentration) in dependence of the dTTP concentrations according to the equation:

$$K_{app} = \left(1+\frac{K_m}{[S]}\right)K_i^{ter} \quad (2)$$

Where K_{app} is the apparent K_i^{ter} at subsaturating substrate concentrations.

The apparent binding rate (k_{app}) values were determined by fitting the experimental data to the single-exponential equation:

$$\left(\frac{v_t}{v_0}\right) = e^{-k_{appt}} \quad (3)$$

where t is time. If $[E]_0$ is the input enzyme concentration, $[E]_t$ is the enzyme available for the reaction at time t and $[E:I]_t$ is the enzyme bound to the inhibitor at time t, it follows that $[E]_t = [E]_0 - [E:I]_t$. Since $v_0 = k_{cat}[E]_0$ and $v_t = k_{cat}[E]_t$, then $v_t/v_0 = 1 - [E:I]_t/[E]_0$. Thus, the v_t/v_0 value is proportional to the fraction of enzyme bound to the inhibitor.

The true association (k_{on}) and dissociation (k_{off}) rates were calculated from the relationships:

$$k_{on} = \frac{k_{app}}{[I]+K_i} \quad \text{and} \quad k_{off} = k_{on}K_i$$

2.8. Antiviral and cytoxicity assays

Evaluation of the antiviral activity and cytoxicity for the PBO derivatives were as described [8,10]. Briefly, a laboratory lymphocyte-tropic strain of HIV-1 (HIV-1-IIIB) was used to infect the C8166 CD4+ T-cell line containing an HTLV-I genome of which only the tat gene is expressed. The antiviral activity of the compounds was assessed by measuring HIV-p24 antigen production in the supernatants of infected cultures by using a commercially available HIV-antigen kit. For toxicity assays, all cell lines were obtained from ATCC. The cells were cultured in RPMI 1640 supplemented with 5% FCS, 0.1 mM glutamine, 1% penicillin, and streptomycin. Cells were grown in Nunc clone plastic bottles (TedNunc, Roskilde, Denmark) and split twice weekly at different cell densities according to standard procedure. 3T3 cells were grown as a monolayer and were split by using tripsin. Perypheral blood mononuclear cells (MNC) were separated from heparinized whole blood obtained from a healthy donor on a Fycoll-Hypaque gradient. MNC thus obtained were washed twice with RPMI 1640 supplemented with 10% FCS, glutamine, and antibiotics, suspended at 200.000 viable cells/ml in medium containing, as mitogen, 5 μg/ml PHA (Sigma) and used in MTT-based toxicity tests. MTT (3-(4,5-dimethylthiazol-2-yl)-2,5-diphenyl-tetrazolium bromide). A total of 20 μl of the 5 mg/mL stock solution of MTT was added to each well; after 2 h of incubation at 37 °C, 100 μl of the extraction buffer was added. After an overnight incubation at 37 °C, the optical densities at 570 nm were measured using a Titer-Tech 96-well multiscanner, employing the extraction buffer as the blank.

2.9. Molecular modeling

All the molecular modeling studies were performed on SGI Indigo II R10000 and SGI Octane 2XR10000 workstations. Compounds (S)-PBO355 and (S)-PBO431 were built using the Insight 2000.1 Builder module. HIV-1 RT crystal structures (PDB IDs: 1RTJ, free form; 1VRT and 1FK9, wild type in complex with nevirapine and efavirenz, respectively; 1RTD, ternary complex; 1HQE, K103N mutant) were downloaded from the PDB data bank (http://www.rcsb.org/pdb/). Hydrogens were added to all the PDB structures considering a pH value of 7.2.

2.9.1. Conformational analysis of compounds (S)-PBO355 and (S)-PBO431

In order to find the global minimum conformer, all the compounds were subjected to a Simulated Annealing procedure. The conformational space of cited compounds was sampled through 50 cycles of Simulated Annealing (Tripos force field, Sybyl software, Tripos, San Louis). A starting temperature of 1000 K was applied to surmount torsional barriers, the structure was equilibrated at that temperature for 1000 fs, then the temperature was reduced to 0 K in 1000 fs, by using an exponential annealing function. Resulting structure

files were transferred in Insight2000.1 package (Accelrys, San Diego) to be subjected to the subsequent MM energy minimization protocol. Atomic potentials and charges were assigned using the CVFF force field. The obtained conformations were geometrically optimized (Discover module, Accelrys, San Diego) using a distance dependent dielectric constant mimicking a protein environment ($\varepsilon = 4 \times r$). Energy minimizations were performed with Conjugate Gradient as minimization algorithm, until the maximum RMS derivative was less than 0.001 kcal/Å. Conformational energy of the proposed bioactive conformations of (S)-PBO355 and (S)-PBO431 has been evaluated through 1 iteration of MM energy minimization ($\varepsilon = 4 \times r$) taking in account the initial energy value.

2.9.2. *Docking studies*

Docking studies were carried out on (S)-PBO355 and (S)-PBO431 [10], using a docking methodology (Affinity, SA_Docking; Insight2000.1, Accelrys, San Diego) which considers all the system (i.e. ligand, protein, and water molecules) flexible. Docking parameters were appropriately tailored to the system on the basis of a series of ''test docking calculation'' performed on 1VRT and 1FK9 crystal complexes. In particular, starting from manually modified initial structures, the parameters able to reproduce the X-ray HIV-1 RT binding modes of nevirapine (1VRT) and efavirenz (1FK9) were chosen. (S)-PBO355 and (S)-PBO431 were docked in to HIV-1 RT X-ray structure of 1VRT, since this latter showed the best resolution among HIV-1 RT crystal structures and the higher degree of solvation of the NNRTI binding site.

To introduce compounds (S)-PBO355 and (S)-PBO431 in the NNBS, nevirapine was removed from the 1VRT crystal structure by using the unmerge command in the Biopolymer Module of Insight2000.1 (Accelrys, San Diego). In order to obtain more representative results, we increased the variance of the docking starting structures. In particular, the pendant phenyl ring pseudo-axial and pseudo-equatorial conformers of (S)-PBO355 and (S)-PBO431 were manually positioned into the NNBS, and both used as starting complexes for the following docking procedure. Moreover, two different energy check criteria, Metropolis and energy test, were adopted for selection of acceptable structures (see below). Each starting complex was subjected to preliminary energy minimization (CVFF force field, Steepest Descent algorithm; $\varepsilon = 1$) until the maximum RMS derivative was less than 0.5 kcal/Å. Indeed, the docking procedure formally requires a reasonable starting structure although in the subsequent flexible docking protocol the complex is perturbed by means of Monte Carlo and Simulated Annealing procedures.

Flexible docking was achieved through the Affinity module in the Insight2000.1 suite, using the SA_Docking procedure and the Cell_Multipole method for non-bond interactions. A binding domain area was defined as a subset including all the residues having at least one atom within 6 Å radius from any given ligand atom. During the entire docking calculations all the atoms included in the defined binding domain area were left free to move, with the exception of water molecules that were tethered with a force constant of 1 kcal/Å^2. A Monte Carlo/minimization approach for random generation of a maximum of 20 structures was used, with an energy tolerance of 10^6 kcal/mol to ensure a wide variance of the input structures to be minimized (2500 iterations; $\varepsilon = 1$). During this step the ligand is moved by a random combination of translation, rotation, and torsional changes, to sample both the conformational space of the ligand and its orientation with respect to the flexible binding domain area. In order to obtain a suitable mobility of water molecules, during this step the tether force applied to water molecules was scaled to a factor of 0.1 (i.e. 10% of its initial value). Similarly, van der Waals (vdW) and Coulombic terms were also scaled to a factor of 0.1 to avoid very severe divergences in the Coulombic and vdW energies. To select acceptable solutions a structure similarity check criterion (RMS tolerance = 0.3 Å) and an energy check criterion were applied. As mentioned above, two different docking procedure were applied on each starting complex, alternatively using as energy check criterion: (i) the energy test (energy range = 50 kcal/mol) or (ii) the Metropolis criterion (temperature = 310 K). Resulting complexes were firstly minimized and then subjected to 50 stages of Simulated Annealing (100 fs each). Over the course of the Simulated Annealing, system temperature was linearly decreased from 500 K to 300 K concurrently the vdW and Coulombic scale factors were similarly decreased from 0.1 to their final values (1.0), while the tether scale factor was kept to 0.1. A final round of 10^6 minimization steps was applied to each complex at the end of the molecular dynamics. After this procedure, the resulting docked complexes were ranked by their conformational energy.

Ligand–enzyme interaction energy of each complex has been evaluated by calculating: (i) the total energy between the ligand and the binding domain area (residues within 6 Å radius from any given ligand atom), using the Evaluate command in the Docking module of Insight2000.1 (vdW and electrostatic energy contribution; no CUT_OFF), (ii) the non-bond interaction energy between the ligand and each protein residues within the binding domain area, using the Discover_3 Module of Insight2000.1 (vdW and electrostatic energy contribution; no CUT_OFF). The lowest energy complexes presenting higher ligand–enzyme interaction energy have been further minimized (CVFF force field, $\varepsilon = 1$) by a combination of Steepest Descent (maximum RMS derivative less than 0.5 kcal/Å) and Conjugate Gradients algorithms (maximum RMS derivative less than 0.1 kcal/Å) and re-subjected to conformational and interaction energy evaluation in order to select the structure representing the most probable binding mode.

The geometry of π–π interactions has been evaluated considering: (i) the distance between the centroids of the aromatic rings, (ii) the angle between the planes of the rings, (iii) the offset value, and (iv) the direction of the dipole vectors.

HIV-1 RT X-ray structures and the docking models of RT in complex with (S)-PBO355 and (S)-PBO431 resulting from docking calculations were superimposed by fitting the backbone atoms of the binding site.

3. Results

3.1. *Steady-state kinetic analysis of the inhibition of HIV-1 RT wild type by optimized PBO derivatives*

We have previously shown that the first-generation PBOs had a novel mechanism of inhibition against HIV-1 RT, since they specifically targeted the catalytically competent ternary

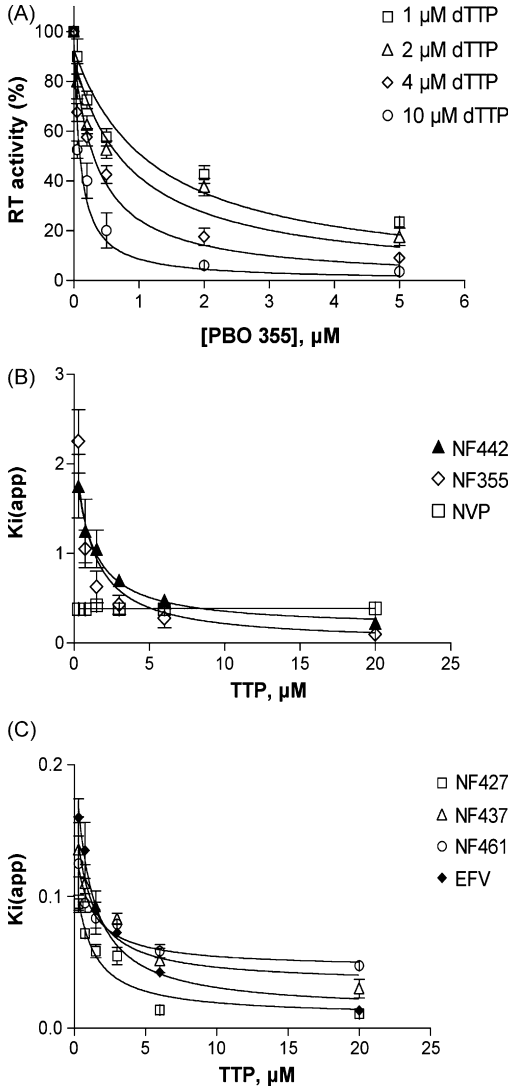

Fig. 2 – Variation of the apparent inhibition constant ($K_{i(app)}$) of nevirapine, efavirenz and PBOs towards HIV-1 RT as a function of the dTTP concentration. Experiments were performed as described in Section 2. (A) Dose–response curves for PBO355 inhibition of HIV-RT wt at various dTTP concentrations. (B) Variation of the $K_{i(app)}$ for NF442 (black triangles), NF355 (diamonds), nevirapine (NVP, squares). (C) Variation of the $K_{i(app)}$ values for NF427 (squares), NF437 (triangles), NF461 (circles) and efavirenz (EFV, black diamonds). The curves in panels B and C were obtained by fitting the $K_{i(app)}$ values calculated from experiments similar to those shown in panel A to Eq. (2). Values represent the mean of three independent replicates. Error bars are ±S.D.

complex of RT with its nucleic acid and nucleotide substrates [9]. As a consequence, their potencies of inhibition were shown to increase as the concentration of the substrates was increased. Thus, we first verified whether our optimized PBO derivatives (Fig. 1) retained the same mechanism of action. HIV-1 RT wild type was challenged with the different inhibitors in the presence of saturating poly(rA)/oligo(dT) and with increasing concentrations of dTTP. The apparent inhibition constants (K_{app}) at increasing dTTP concentrations for all the different inhibitors were then determined, as shown in Fig. 2A for PBO 355, and their variation in dependence of the nucleotide substrate concentrations is shown in Fig. 2B and C. All the inhibitors tested showed an increase in potency (reduction of K_{app} values), which was dependent on the dTTP concentrations. From these data it was possible to calculate the true dissociation constant (K_i^{ter}) for binding of each inhibitor to the ternary complex between the enzyme and its substrates nucleic acid and dNTP. The derived values are listed in Table 1. In order to calculate the apparent equilibrium dissociation constants for the interaction of the inhibitors with the free enzyme (K_i^{free}) and the binary RT/template–primer (TP) complex (K_i^{bin}), the inhibition of HIV-1 RT wt by the different PBO derivatives was analysed as a function of both the nucleic acid and the nucleotide substrates. According to the ordered mechanism of the polymerization reaction, whereby TP binds first followed by addition of deoxynucleotide triphosphate (dNTP), the HIV-1 RT can be present in three different catalytic forms: as a free enzyme, in a binary complex with the TP and in a ternary complex with TP and dNTP. The steady-state kinetic analysis was simplified by varying one of the substrates (either TP or dNTP) while the other was kept constant. Thus, when the TP substrate was held constant at saturating concentration and the inhibition analyzed in dependence of varying concentrations of dNTPs, at the steady-state all the input RT was in the form of the RT/TP binary complex and only two forms of the enzyme (the binary complex and the ternary complex with dNTP) could react with the inhibitor. Similarly, when the dNTP concentration was kept constant at saturating levels and the inhibition analyzed in dependence of varying TP concentrations, RT was present either as a free enzyme or in the ternary complex with TP and dNTP. Complex formation between RT and its substrates was assumed to occur with rapid equilibrium kinetics, so in the presence of saturating dNTP, the conversion of the binary RT/TP complex into a ternary complex was assumed to occur at a much faster rate than inhibitor binding. Thus, in both cases simple steady-state kinetic analysis could be used for the determination of the equilibrium dissociation constants K_i^{free} and K_i^{bin} (see Section 2) for the different enzyme–inhibitor complexes. As reported in Table 1, for all the inhibitors tested K_i^{free} values were close to those of K_i^{bin}, whereas K_i^{ter} values were significantly lower. These data clearly indicated a higher affinity of the PBO derivatives for the catalytically competent ternary complex of HIV-1 RT.

3.2. *Selective targeting of the ternary complex of the drug-resistant RT mutant K103N by PBO derivatives*

The analysis described above was extended to selected HIV-1 RT mutants carrying the NNRTIs-resistance mutations L100I, K103N, V179D and Y181I. As can be seen by the corresponding values for K_i^{free}, K_i^{bin} and K_i^{ter} (Table 1), all the tested compounds showed the same mechanism of action against these mutants as reported for RT wild type, namely the selective targeting of the ternary complex of RT with its substrates. In order to investigate the effects of the selected mutations on the selectivity of the inhibitors tested for the ternary complex,

Table 1 – Kinetic parameters for drugs binding to RT wild type and the K103N, L100I and V179D mutants

	[E]			[E:DNA]			[E:DNA:dNTP]		
	K_i^{free} (μM)	k_{on} ($s^{-1} M^{-1}$) × 10^{-4}	k_{off} (s^{-1}) × 10^4	K_i^{bin} (μM)	k_{on} ($s^{-1} M^{-1}$) × 10^{-4}	k_{off} (s^{-1}) × 10^4	K_i^{ter} (μM)	k_{on} ($s^{-1} M^{-1}$) × 10^{-4}	k_{off} (s^{-1}) × 10^4
Wild type									
PBO355	1.5 ± 0.1	0.3 ± 0.05	45 ± 5	1.5 ± 0.2	0.16 ± 0.03	25 ± 3	0.08 ± 0.01	0.37 ± 0.05	3 ± 0.4
PBO427	0.12 ± 0.02	0.4 ± 0.1	5 ± 0.6	0.1 ± 0.02	0.8 ± 0.1	8.5 ± 0.5	0.039 ± 0.006	6.4 ± 0.4	2 ± 0.3
PBO442	1.5 ± 0.2	0.3 ± 0.05	45 ± 5	1.7 ± 0.3	0.16 ± 0.03	27 ± 3	0.3 ± 0.06	0.1 ± 0.02	3 ± 0.5
PBO461	0.2 ± 0.04	0.2 ± 0.05	4.4 ± 0.04	0.26 ± 0.05	0.8 ± 0.1	21 ± 3	0.05 ± 0.01	10 ± 1	50 ± 5
PBO431	0.15 ± 0.02	0.1 ± 0.02	1.5 ± 0.02	0.16 ± 0.03	0.12 ± 0.02	2 ± 0.3	0.067 ± 0.002	0.6 ± 0.1	4 ± 0.5
PBO437	1 ± 0.2	0.1 ± 0.02	10 ± 1	1 ± 0.1	0.09 ± 0.01	11 ± 1	0.6 ± 0.1	0.4 ± 0.05	24 ± 2
EFV	0.17 ± 0.02	0.1 ± 0.02	1.7 ± 0.2	0.03 ± 0.004	1.3 ± 0.1	4 ± 0.5	0.01 ± 0.001	1.4 ± 0.3	1.6 ± 0.2
NVP	0.4 ± 0.05	0.15 ± 0.02	6 ± 1	0.3 ± 0.02	0.2 ± 0.02	6 ± 1	0.3 ± 0.03	0.2 ± 0.02	6 ± 1
K103N									
PBO355	6 ± 1	0.006 ± 0.001	4 ± 0.5	11 ± 1	0.009 ± 0.001	12 ± 1	0.09 ± 0.01	0.66 ± 0.06	6 ± 0.6
PBO427	n.d[a]	n.d.	n.d.	n.d	n.d.	n.d.	n.d.	n.d.	n.d.
PBO442	75 ± 5	0.026 ± 0.005	195 ± 5	70 ± 3	0.05 ± 0.01	370 ± 20	2.3 ± 0.3	0.013 ± 0.002	31 ± 2
PBO461	10 ± 1	0.003 ± 0.0006	3 ± 0.4	10 ± 1	0.004 ± 0.001	4 ± 0.6	0.2 ± 0.03	0.062 ± 0.002	12 ± 1
PBO431	13 ± 1	0.007 ± 0.001	9 ± 1	14 ± 1	0.009 ± 0.001	12 ± 1	0.3 ± 0.05	0.3 ± 0.06	8.5 ± 0.5
PBO437	10 ± 1	0.003 ± 0.0006	3 ± 0.5	10 ± 1	0.004 ± 0.001	4 ± 0.5	2 ± 0.3	0.25 ± 0.03	50 ± 5
EFV	n.d.			n.d.			0.2 ± 0.02	0.6 ± 0.1	12 ± 1
NVP	6.6 ± 0.3	0.015 ± 0.002	10 ± 1	6.6 ± 0.3	0.015 ± 0.002	10 ± 1	6.6 ± 0.3	0.015 ± 0.002	10 ± 1
L100I									
PBO355	3 ± 0.4	0.6 ± 0.1	175 ± 5	3.5 ± 0.3	0.4 ± 0.05	120 ± 10	0.12 ± 0.02	1.1 ± 0.1	14 ± 1
PBO427	3 ± 0.4	0.6 ± 0.1	180 ± 5	3.2 ± 0.3	0.38 ± 0.05	120 ± 10	1.5 ± 0.2	1.2 ± 0.1	112 ± 10
PBO442	7 ± 1	0.3 ± 0.05	210 ± 10	15 ± 1	0.13 ± 0.03	205 ± 10	4 ± 0.5	0.01 ± 0.002	59 ± 4
PBO461	2.5 ± 0.3	0.1 ± 0.02	25 ± 2	2 ± 0.3	0.17 ± 0.02	35 ± 2	0.2 ± 0.03	0.8 ± 0.1	16 ± 1
PBO431	1.5 ± 0.2	0.06 ± 0.01	8.7 ± 0.5	1.6 ± 0.2	0.05 ± 0.01	7 ± 1	0.15 ± 0.03	1.4 ± 0.2	21 ± 1
PBO437	15 ± 1	0.13 ± 0.02	205 ± 10	7 ± 1	0.3 ± 0.04	210 ± 10	0.7 ± 0.1	2 ± 0.03	140 ± 10
V179D									
PBO355	10 ± 1	0.025 ± 0.02	25 ± 2	12 ± 1	0.02 ± 0.003	24 ± 2	0.8 ± 0.1	0.4 ± 0.03	31 ± 2
PBO427	5 ± 0.3	0.06 ± 0.01	29 ± 2	8 ± 1	0.1 ± 0.02	80 ± 5	0.8 ± 0.1	0.4 ± 0.05	32 ± 2
PBO442	20 ± 2	0.04 ± 0.005	86 ± 6	25 ± 2	0.035 ± 0.005	87 ± 7	2.5 ± 0.3	0.03 ± 0.006	16.5 ± 0.5
PBO461	7 ± 1	0.15 ± 0.02	103 ± 10	7 ± 1	0.07 ± 0.01	50 ± 2	0.3 ± 0.04	1.2 ± 0.2	40 ± 2
PBO431	9 ± 1	0.03 ± 0.006	28 ± 2	11 ± 1	0.02 ± 0.004	23 ± 2	0.25 ± 0.03	1 ± 0.1	25 ± 0.2
PBO437	20 ± 2	0.05 ± 0.01	100 ± 10	20 ± 2	0.04 ± 0.01	80 ± 10	2.5 ± 0.2	0.03 ± 0.004	16.5 ± 0.5
Y181I									
PBO427	10 ± 1	0.07 ± 0.01	70 ± 8	12 ± 1	0.05 ± 0.007	60 ± 6	1.2 ± 0.1	0.5 ± 0.06	60 ± 5
PBO431	8 ± 1	0.02 ± 0.003	16 ± 1	6 ± 0.6	0.03 ± 0.004	20 ± 2	0.5 ± 0.06	0.5 ± 0.06	25 ± 2

[a] n.d., not determined, the compound was inactive at the highest tested concentration. Values are the means of three replicates ± S.D.; EFV, efavirenz; NVP, nevirapine.

the K_i^{free} and K_i^{bin} values obtained with RT wild type and the mutants were compared to the corresponding K_i^{ter} values, and their fold decrease (reflecting the increased affinity of the inhibitors for the ternary complex) was calculated. The results are shown in the form of bar plots for each of the tested compounds (Fig. 3). As shown, all the inhibitors displayed a significant increase in the affinity for the ternary complex with respect to both the free enzyme and the binary complex, for all the enzyme tested. Interestingly, PBO355, the most active compound against K103N mutant, showed the greatest increase in affinity for the RT wild type ternary complex ($K_i^{free}/K_i^{ter} = 19$). These results seem to account for the similarity in the primer grip region (W229) between the X-ray structures of RT wt ternary complex and the K103N mutant (Fig. 5A and Fig. 5C vs Fig. 5D). Moreover, the overall highest selectivity toward the ternary complex is observed for K103N (Table 1) and resulted to be correlated to the K_i value for this mutant [10]. In particular, the compounds PBO437, PBO442, PBO431, PBO461 and PBO355, showed an increased affinity (decrease of their K_i values) for the ternary complex with respect to the free enzyme, of 5-, 33-, 43-, 50- and 67-fold, respectively, in the case of the mutant K103N, whereas the corresponding increase for the wild type RT was 1.7-, 5-, 2.2-, 4- and 19-fold, respectively. The highest decrease of the K_i value for the ternary complex with respect to the free enzyme for the mutant L100I was achieved by PBO355 and PBO437 (25- and 21-fold, respectively), whereas PBO431 scored better than the other inhibitors in the case of the mutant V179D (16-fold decrease in K_i for the ternary complex with respect to the free enzyme). The PBO355 derivative remained the most active compound against the K103N and L100I mutants, however PBO461 and PBO431 displayed increased activities against the mutant V179D (Table 1). This increased activity correlated with an increased affinity of these two compounds for the ternary complex of the V179D mutated enzyme (23- and 36-fold, respectively), with respect to PBO355 (12.5-fold). Only two compounds (PBO427 and PBO431) displayed significant

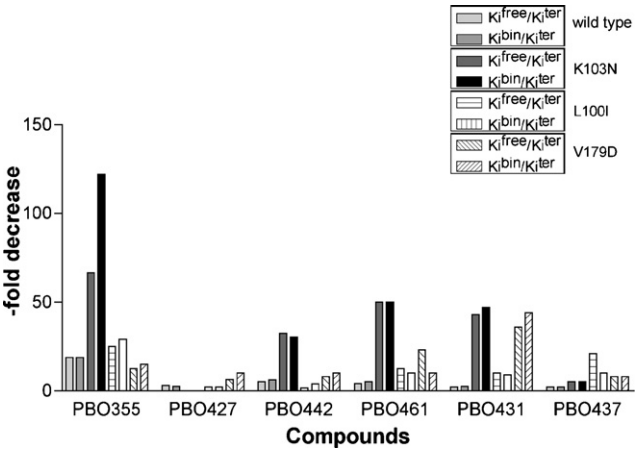

Fig. 3 – The PBO derivatives showed an increased affinity towards the ternary complex of HIV-1 RT wild type and mutants. The equilibrium dissociation constants for the free enzyme (K_i^{free}), the binary (K_i^{bin}) and the ternary (K_i^{ter}) complexes were determined as described in Section 2. The ratios between the K_i^{free} and K_i^{ter} or K_i^{bin} and K_i^{ter}, representing the increase in affinity from the free enzyme and the binary complexes to the ternary complex, respectively, were calculated from the values reported in Table 1. Values are plotted as fold decrease in the respective K_i values for the different enzymes tested in the presence of PBO355, PBO427, PBO442, PBO437, PBO431 and PBO461.

activity towards the Y181I mutant, with PBO431 being the most active. Analysis of the binding of these inhibitors to the different catalytic forms of the Y181I enzyme showed that both compounds retained the specificity for the ternary complex of the mutated enzyme (K_i decrease: PBO427, 8-fold; PBO431, 16-fold) which was due to an increase in the association rates (k_{on}) with respect to the apoenzyme or the binary complex (Table 1). Resistance was achieved mainly through an increased dissociation rate of the inhibitor from the ternary complex of the mutated enzyme with respect to HIV-1 RT wild type (Table 1). However, this increase was strongly reduced by the introduction of the extended aromatic group at position C-6 in PBO431 (6-fold), with respect to PBO427 (10-fold). These results indicate a specific targeting of the ternary complex of wild type and mutant RTs by PBOs, with a clear cut selectivity for the ternary complex of the K103N mutant for the compounds that target the primer grip (W229), in agreement with our previous docking studies results [10]. Moreover, optimized PBOs proved to possess a broader spectrum of activity. The antiviral activity and cytoxicity profile of these compounds was also very promising (Table 2). In particular, PBOs proved to have extremely low toxicity (TC_{50}) on a variety of human and murine cell lines.

3.3. *Different contributions of the inhibitor association and dissociation rates to the selective targeting by PBOs of the ternary complex of HIV-1 RT wild type and mutants*

In principle, a higher affinity of an inhibitor for a given enzymatic form could result from either an increased association rate, or a decreased dissociation rate, or both. In order to elucidate the mechanism driving the specific targeting of the RT ternary complex by PBOs, equilibrium binding experiments were performed (see Section 2) in order to determine the association (k_{on}) or dissociation (k_{off}) rates for all the inhibitors to the different RT forms (free enzyme, binary complex and catalytically competent ternary complex) along the enzyme's reaction pathway, with HIV-1 RT wild type and the L100I, K103N, V179D and Y181I mutants. The calculated k_{on} and k_{off} values (Table 1) for the binary and ternary complexes were then compared to the corresponding values for the free enzyme.

The increase in the association rates from the free enzyme to the ternary complex is shown in Fig. 4A, in the form of bar plots. The compound PBO355 showed a large increase only in the association rate to the ternary complex of the mutants K103N and, to a lesser extent, V179D. The compound PBO427, showed a 20-fold increased association rate to the ternary complex of RT wild type, with respect to the other enzymatic forms, and only a modest increase to the mutant V179D. Remarkably, PBO442 did not show an increased association rate to the ternary complex of any of the enzymes tested. PBO431 showed an increase in the association rate to the ternary complex of all the enzyme tested, with higher specificity for the mutated forms L100I, K103N, V179D (23-, 33- and 42-fold increase) with respect to RT wild type (6-fold increase). Compound PBO437 similarly showed an increase in the association rate to the ternary complex of all the enzyme tested, with the exception of the mutant V179D, presenting the highest specificity for the K103N mutant. The PBO461 derivative, showed the highest increase in the association rate to the ternary complex of RT wild type (almost 50-fold), although this specificity was reduced by the mutations L100I,

Table 2 – Antiviral activity and cytoxicity of PBOs in different cell lines infected by HIV-1_{IIIB}

Compound	C8166[a]			NSO	DH	3T3F	HL
	EC_{50}[b] (μM)	CC_{50} (μM)	S.I.	TC_{50} (μM)			
PBO355	0.4	52	130	>1000	>1000	>1000	>1000
PBO461	0.5	11	22	720	740	700	720
PBO431	0.08	10	125	800	850	820	810

[a] C8166, lymphocytic CD4+ T-cell line; NSO, murine cell line; DH, Daudi human cell line; 3T3F, murine fibroblast cell line; HL, normal human lymphocytes.

[b] EC_{50}, dose reducing 50% the survival of infected cells compared to the uninfected control; CC_{50}, dose reducing 50% the survival of uninfected cells; S.I., selectivity index calculated as CC_{50}/EC_{50}; TC_{50}, drug resulting in 50% cytotoxicity in MTT assays. Data from refs. [8,10].

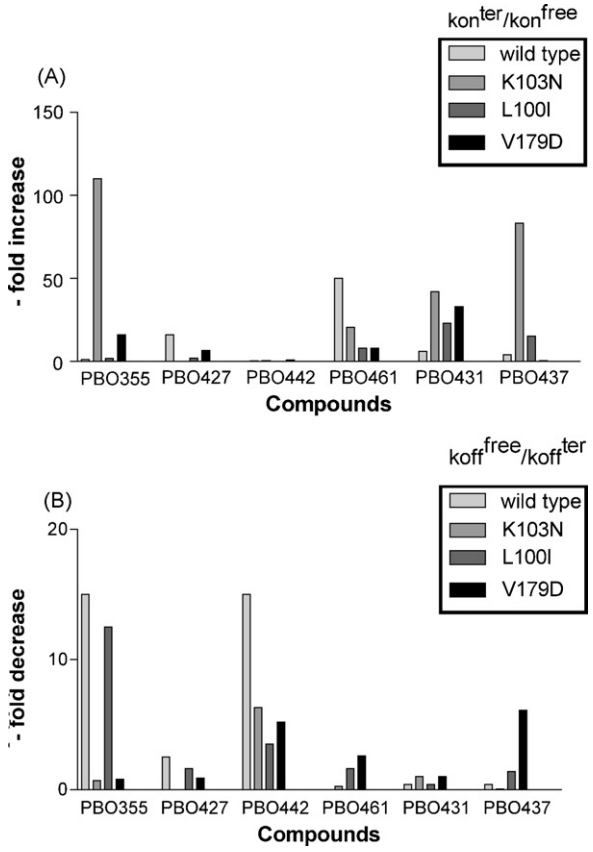

Fig. 4 – Variation of the association (k_{on}) and the dissociation (k_{off}) rates of the PBOs for the ternary complex of HIV-1 RT wild type and mutants with respect to the free enzyme. (A) The association rates (k_{on}) values for binding of the inhibitors to the different enzymatic forms were calculated as described in Section 2 and listed in Table 1. The ratios between the k_{on} rates for the binary (light grey) and ternary (dark grey) complexes of wild type and mutated RTs and the corresponding value for the free enzyme, were computed and plotted (as fold increase) for PBO355, PBO427, PBO442, PBO431, PBO437 and PBO461. B. The dissociation rates (k_{off}) values for binding of the inhibitors to the different enzymatic forms were calculated as described in Section 2 and listed in Table 1. The ratios between the k_{off} value for the free enzyme and the corresponding rates for the binary (light grey) and ternary (dark grey) complexes of wild type and mutated RTs, were computed and plotted (as fold decrease) for PBO355, PBO427, PBO442, PBO431, PBO437 and PBO461.

K103N and V179D (8-, 20- and 10-fold increase, respectively). None of the compounds showed any significant increase in their association rates to the binary complex, with respect to the free enzyme (Table 1), confirming their high selectivity for the ternary complex of RT with its substrates.

The same analysis was performed by evaluating the decrease in the dissociation rates (k_{off}) of the various inhibitors from the ternary complexes of wild type and mutated RT, with respect to the free enzyme. The results are shown in Fig. 4B. The compounds PBO355 and PBO427 showed a decrease in the dissociation rates for RT wild type and the L100I mutant, whereas the compound PBO442, showed a decrease in its dissociation rate from the ternary complex with all the enzyme tested. None of the other compounds showed any significant variation in their k_{off} rates, with the exceptions of PBO461 (10-fold increase in the k_{off} value for RT wild type) and PBO437 (17-fold increase in the k_{off} value for the V179D). Also, all the tested PBOs did not show any variation in their k_{off} values for the binary complex (Table 1).

By comparing the results presented in Fig. 4A and 4B, it was possible to make some considerations on the molecular basis for the observed selectivity for the ternary complex of the compounds analysed. For example, PBO355 achieved selectivity for the ternary complexes of RT wt and the mutant L100I through an increased stability (lower k_{off} values, Fig. 4B), whereas binding to the ternary complex of the mutants K103N and V179D was due to an increased association rate (Fig. 4A). The two extreme cases were those of the compound PBO431, showing the overall better activity on the tested mutants, whose selective targeting of the ternary complex was solely driven by an increase in the association rate with all the enzymes tested, and of PBO442, which showed exactly the opposite behaviour (compare Fig. 4A and B). In general, the optimized PBO derivatives characterized by an extended aromatic system at C-6 (i.e. PBO431, PBO437, and PBO461) improved their selectivity for the ternary complex mainly increasing the association rate constant according to our hypothesized enhanced interaction with W229 (Fig. 5F) [10].

3.4. *Novel PBOs display lower susceptibility towards drug-resistant RT mutants than nevirapine and efavirenz*

The K_i^{ter} values reported in Table 1 were used to calculate the relative resistance indexes (K_i^{mut}/K_i^{wt}), which are listed in Table 3 along with the corresponding values for the different first- and second-generation NNRTIs efavirenz and nevirapine, respectively. All the compounds showed a significantly better activity spectrum than nevirapine and much lower sensitivity to the K103N mutation than efavirenz. In particular, the compound PBO355 showed the lowest sensitivity towards the K103N mutation among the inhibitors tested and a moderate sensitivity towards the V179D mutant (10-fold). Compounds PBO431, PBO437 and PBO461, which specifically target the primer grip region, showed similar low sensitivities towards the mutants L100I, K103N and V179D (in the range of 1.2- to 6-fold). According to our hypothesised binding mode [10], the most affected compounds were PBO427 and PBO442, which showed high-level sensitivity towards all mutants. The derivatives PBO427 and PBO431 were the only ones active towards the Y181 mutant (Table 1). However, as can be seen from the data in Table 3, the extended aromatic system at C-6 of PBO431 resulted in a 4-fold improved selectivity towards this mutant.

3.5. *Structural comparison of HIV-1 RT free form, ternary complex and K103N mutant and docking results of PBO355 and PBO431 in complex with HIV-1 RT free form*

We compared the structures of the ternary complex, which is specifically targeted by the PBOs, with the one of the apoenzymatic form of wild type and K103N RT (Fig. 5A–D). As

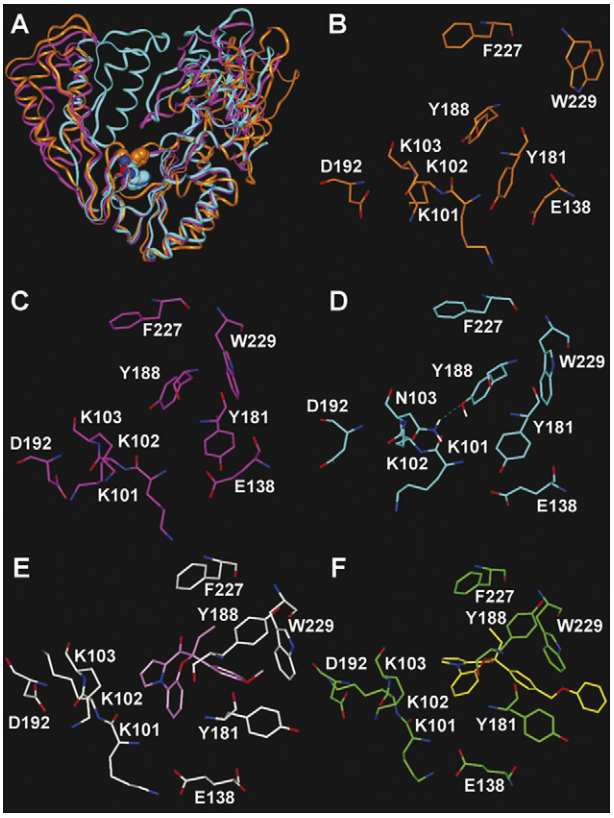

Fig. 5 – Structural comparison of HIV-1 RT free form, ternary complex and K103N mutant and docking results of PBO355 and PBO431 in complex with HIV-1 RT free form. (A) Superimposition of the X-ray structures of RT thumb, palm and finger domains: free form (orange), ternary complex (magenta) and K103N mutant (cyan). RTs are displayed as ribbons, Van der Waals volume of W229 is evidenced. Zoom of RT-NNBS of free form (B), of ternary complex (C) and of K103N mutant (D). (E) Compound PBO355 (pink) docked into the HIV-1 RT (white). (F) Compound PBO431 (yellow) docked into the HIV-1 RT (green). All molecules are colored by atom type (O = red; N = blue; H = white). Hydrogen bonds are highlighted by green dashed lines. Hydrogen are omitted for sake of clarity, with the exception of those involved in hydrogen bond interactions.

shown in Fig. 5A, superimposition of the three structures revealed a larger degree of overlapping between the NNBSs of the ternary complex (magenta) and the K103N free RT (cyan), with respect to the free wild type enzyme (orange). In particular, in the ternary complex the residue W229 is oriented as in the K103N mutant apoenzyme (Fig. 5C vs Fig. 5D). On the basis of these results, we investigated the role played by the interaction of PBOs with the primer grip region (W229) for the selectivity towards the K103N and the ternary complex. To this purpose, we took into account flexible docking studies previously reported by us on the derivatives PBO355 and PBO431 into the structure of the HIV-1 RT free form [10] (Fig. 5E and F). The docking approach used allows the mutual adaptability of the ligand with respect to the binding site

Table 3 – Relative resistance values (fold, $K^{ter}_{i\,mut}/K^{ter}_{i\,wt}$) for PBOs, nevirapine and efavirenz towards common NNRTIs-resistant mutants

Compound	Enzyme			
	L100I	K103N	V179D	Y181I
PBO355	1.5	1.1	10	n.a.[a]
PBO427	38.5	n.a.	20.5	30.8
PBO442	13.3	7.7	8.3	n.a.
PBO431	2.2	4.5	3.7	7.5
PBO461	4	4	6	n.a.
PBO437	1.2	3.3	4.2	n.a.
NVP[b]	40	22	50	50
EFV[c]	5	20	5	30

[a] n.a., not applicable, the inhibitor was not active against the mutant.
[b] NVP, nevirapine.
[c] EFV, efavirenz.

around the inhibitor, considering both the inhibitor and the NNBS fully flexible during the calculations. Interestingly, as shown in Fig. 5E and F, both the PBO355 and the PBO431 resulted to be able to strongly interact with W229. In particular, the methoxyphenyl ring of PBO355 is positioned in the aromatic cleft lined by Y181 and Y188, and establishes π–π interactions with the side chain of W229 (Fig. 5E). PBO431 has an extended aromatic system at C-6 (Fig. 5F). Docking of this compound shows that the phenyloxymethyl substituent of the pendant phenyl ring at C-6 further extends the contact region with W229, resulting in additional and more stable contacts. This increased stability allowed also to improve the activity of PBO355 and PBO431 against the mutant enzymes and, particularly, the K103N (Tables 1 and 2). Interestingly, although PBO355 and PBO431 were docked in to the NNBS of RT wt free form (Fig. 5B), in the resulting docked complex (Fig. 5E and F) the position adopted by W229 ended to be similar to that adopted in the RT wt ternary complex and in the K103N mutant (Fig. 5C and D).

4. Discussion

The compounds presented here belong to two different sets. The lead compounds PBO355, 427, 442 and the rationally optimized PBO431, 437, 461. They have been shown to potently suppress HIV-1 replication in cell culture (Table 2 and ref. [10]). The majority of NNRTIs act as purely non-competitive inhibitors, that is they do not discriminate between the different catalytic forms of the enzyme. A notable exception is efavirenz, which has been previously described by us to show an increased affinity for the binary and ternary complexes with respect to the free RT (Table 1 and ref. [15]). Indeed, efavirenz shows a better activity profile than nevirapine against several drug-resistant mutants. Previous biochemical studies on PBOs mode of action demonstrated a preferential targeting of the ternary complex of HIV-1 RT with its substrates. This observation led to the hypothesis that, since the conformation of the NNRTI binding site, in particular W229, of the docked complex of PBO/wt-RT is very similar to both the conformation of K103N mutant NNRTI binding site

and to the one of the ternary complex of RT and its substrates (Fig. 5), PBOs should show a selective binding to both the ternary complex and the K103N mutant. In order to prove this hypothesis, we have selected the compounds studied in the present paper to be tested for their affinity for the different forms of the wt and mutant enzymes.

In summary, the results of our biochemical studies clearly indicated that: (i) all the active PBO derivatives displayed a significant increase in the affinity for the ternary complex of RT, either wild type or carrying NNRTI-resistance mutations, with respect to both the free enzyme and the binary complex; (ii) all the compounds active against K103N mutant [10] showed a high increase in affinity for the ternary complex of this mutant as shown by their K_i values; (iii) PBOs selectivity was improved through specific interaction with the primer grip region (W229), and was achieved either through an increased association or to a decreased dissociation rate. In particular, PBO355, showing the highest activity on the K103N mutant and the highest selectivity toward the ternary complex of this mutant (65-fold, exclusively due to an increased association rate), displayed also the higher ratio between K_i^{free}/K_i^{ter} for wild type RT, resulting in a 19-fold increase in inhibition toward the ternary complex of the enzyme (Table 1). The molecular and structural basis for this correspondence between the specificity for the ternary complex of the wild type RT and the increased selectivity towards the K103N mutant have been investigated through molecular modeling studies. The major difference that arises at the NNBS (non-nucleoside binding site) level due to the K103N mutation with respect to HIV-1 RT free form is that the W229 side chain reorients towards the Y181 and Y188 side chains, and the latter establishes a hydrogen bond with the mutated N103 side chain. It is also known, however, that extensive rearrangements occur in the HIV-1 RT structure upon binding of the substrates, so that the free enzyme is not structurally equivalent to the binary or ternary complex [16]. The compounds were docked in the free form of the enzyme with the aim to provide a computational support to our hypothesis that the complex between the ligand and the ternary form of the enzyme is the most stable one, in terms of enthalpy and entropy. We performed a dynamic docking procedure in which the molecules are fully free to rearrange on the bases of their non-bond interactions (i.e. binding energy) and of the Boltzman factor, thus resulting in the formation of the thermodynamically most stable ligand/enzyme complex. In this view, the fact that our calculations showed that, even starting from the ''free form conformation'' of the active site of the enzyme (and considering different ligand conformers), the binding with the ligand always stabilized the ''ternary complex conformation'', suggests that both the specific targeting of the ternary complex and the selectivity towards the K103N mutation rely on the ability of PBOs to establish strong interactions with the W229 side chain, which allow to more easily penetrate the NNBS. Moreover, the stabilizing interaction with W229 can compensate the effects of other mutations (L100I, V179D and Y181I). Thus, targeting the interaction with W229 appears an useful approach for increasing the activity of PBOs towards NNRTIs-resistant mutants and to selectively target the ternary complex of the enzyme. The nature of the substituents at C-6 appears critical for modulating the rate of association of the PBO inhibitors to the different mutants. The validity of such approach is demonstrated by the improved activity of some of the optimized PBOs against the mutants with respect to the first-generation compounds (Table 1). The activity spectrum was also improved in some cases, as shown by the relative resistance indexes of PBO431 against the mutants V179D and Y181I (Table 3). PBO431 was also the most active compound in inhibiting HIV-1 replication in cell culture and showed a very promising toxicity profile against various cell lines (Table 2). Thus, further structure–activity and molecular modelling studies on PBOs are warranted to develop compounds endowed with high antiviral potency and broad activity spectrum against the most common drug-resistant RT mutants.

Acknowledgments

We thank Dr. Alberto Bergamini, University of Rome-Tor Vergata, for his contribution to the generation of the antiviral and cytotoxicity data. GM was partially supported by the Istituto Superiore di Sanità-National Program on AIDS, Contract 40G.36. S.Z. is the recipient of a Buzzati-Traverso fellowship. The Authors declare no conflict of interests.

REFERENCES

[1] De Clercq E. Non-nucleoside reverse transcriptase inhibitors (NNRTIs): past, present, and future. Chem Biodivers 2004;1:44–64.
[2] Balzarini J. Current status of the non-nucleoside reverse transcriptase inhibitors of human immunodeficiency virus type 1. Curr Top Med Chem 2004;4:921–44.
[3] Rivero A, Mira JA, Pineda JA. Liver toxicity induced by non-nucleoside reverse transcriptase inhibitors. J Antimicrob Chemother 2007;59:342–6.
[4] Vella S, Palmisano L. Antiretroviral therapy: state of the HAART. Antivir Res 2000;45:1–7.
[5] Richman D, Shih C-K, Lowy I, Rose J, Prodanovich P, Goff S, et al. Human immunodeficiency virus type 1 mutants resistant to nonnucleoside inhibitors of reverse transcriptase arise in tissue culture. Proc Natl Acad Sci USA 1991;88:11241–5.
[6] Boone LR. Next-generation HIV-1 non-nucleoside reverse transcriptase inhibitors. Curr Opin Invest Drugs 2006;7:128–35.
[7] Zhou Z, Lin X, Madura JD. HIV-1 RT nonnucleoside inhibitors and their interaction with RT for antiviral drug development. Infect Disord Drug Targets 2006;6:391–413.
[8] Campiani G, Morelli E, Fabbrini M, Nacci V, Greco G, Novellino E, et al. Pyrrolobenzoxazepinone derivatives as non-nucleoside HIV-1 RT inhibitors: further structure-activity relationship studies and identification of more potent broad-spectrum HIV-1 RT inhibitors with antiviral activity. J Med Chem 1999;42:4462–70.
[9] Locatelli GA, Campiani G, Cancio R, Morelli E, Ramunno A, Gemma S, et al. Effects of drug resistance mutations L100I and V106A on the binding of pyrrolobenzoxazepinone nonnucleoside inhibitors to the human immunodeficiency virus type 1 reverse transcriptase catalytic complex. Antimicrob Agents Chemother 2004;48:1570–80.

[10] Fattorusso C, Gemma S, Butini S, Huleatt P, Catalanotti B, Persico M, et al. Specific targeting highly conserved residues in the HIV-1 reverse transcriptase primer grip region. Design, synthesis, and biological evaluation of novel, potent, and broad spectrum NNRTIs with antiviral activity. J Med Chem 2005;48:7153–65.
[11] Pelemans H, Esnouf R, De Clerq E, Balzarini J. Mutational analysis of Trp-229 of human immunodeficiency virus type 1 reverse transcriptase (RT) identifies this amino acid residue as a prime target for the rational design of new non-nucleoside RT inhibitors. Mol Pharmacol 2000;57:954–60.
[12] Wohrl BM, Krebs R, Thrall SH, Le Grice SF, Scheidig AJ, Goody RS. Kinetic analysis of four HIV-1 reverse transcriptase enzymes mutated in the primer grip region of p66 implications for DNA synthesis and dimerization. J Biol Chem 1997;272:17581–7.
[13] Boyer PL, Ferris AL, Clark P, Whitmer J, Frank P, Tantillo C, et al. Mutational analysis of the fingers and palm subdomains of human immunodeficiency virus type-1 (HIV-1) reverse transcriptase. J Mol Biol 1994;243:472–83.
[14] Maga G, Amacker M, Ruel N, Hubscher U, Spadari S. Resistance to nevirapine of HIV-1 reverse transcriptase mutants: loss of stabilizing interactions and thermodynamic or steric barriers are induced by different single amino acid substitutions. J Mol Biol 1997;274:738–47.
[15] Maga G, Ubiali D, Salvetti R, Pregnolato M, Spadari S. Selective interaction of the human immunodeficiency virus type 1 reverse transcriptase nonnucleoside inhibitor efavirenz and its thio-substituted analog with different enzyme-substrate complexes. Antimicrob Agents Chemother 2000;44:1186–94.
[16] Huang H, Chopra R, Verdine GL, Harrison SC. Structure of a covalently trapped catalytic complex of HIV-1 reverse transcriptase: implications for drug resistance. Science 1998;282:1669–75.